



# CHORUS

This is the accepted manuscript made available via CHORUS. The article has been published as:

## Dynamics of a Compound Vesicle in Shear Flow

Shravan K. Veerapaneni, Y.-N. Young, Petia M. Vlahovska, and Jerzy Bławdziewicz

Phys. Rev. Lett. **106**, 158103 — Published 14 April 2011

DOI: [10.1103/PhysRevLett.106.158103](https://doi.org/10.1103/PhysRevLett.106.158103)

## Dynamics of a compound vesicle in shear flow

Shravan K. Veerapaneni<sup>1</sup>, Y.-N. Young<sup>2</sup>, Petia M. Vlahovska<sup>3</sup> and Jerzy Bławdziewicz<sup>4</sup>

<sup>1</sup>*Courant Institute of Mathematical Sciences, NYU, New York, NY 10012, USA*

<sup>2</sup>*Department of Mathematical Sciences, NJIT, Newark, NJ 07102, USA*

<sup>3</sup>*School of Engineering, Brown University, Providence, RI 02906, USA*

<sup>4</sup>*Department of Mechanical Engineering, Texas Tech University, Lubbock, TX 79409, USA*

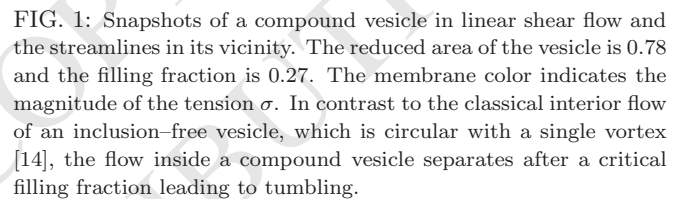
The dynamics of a compound vesicle (a lipid bilayer membrane enclosing a fluid with a suspended particle) in shear flow is investigated using both numerical simulations and theoretical analysis. We find that the non-linear hydrodynamic interaction between the inclusion and the confining membrane gives rise to new features of the vesicle dynamics: Transition from tank-treading to tumbling can occur in the absence of any viscosity mismatch, and a vesicle can swing if the enclosed particle is non-spherical. Our results highlight the complex effects of internal cellular structures have on cell dynamics in microcirculatory flows. For example, parasites in malaria-infected erythrocytes increase cytoplasmic viscosity, which leads to increase in blood viscosity.

PACS numbers: 87.16.dm,47.63.mf,83.50.Ax,47.57.Qk

The biological cell is, in essence, a lipid bilayer membrane encapsulating the cellular content. Giant vesicles made of lipid membrane serve as simple cell mimics [1], especially for the red blood cell (RBC) [2]. Under shear flow, vesicles and RBCs display two main types of dynamics: tank-treading (TT) and tumbling (TB) [3–5]. Vesicles also display a vacillating-breathing motion (VB) (also called trembling [4] and swinging [6]), in which the vesicle long axis oscillates about the shear direction while the shape undergoes strong deformation. Theoretical analyses highlighted the membrane area-incompressibility as the source of the non-linear dynamics [7]; unlike vesicles, droplets do not tumble in shear flow. Moreover, for a vesicle with a given area-to-volume ratio, the mismatch between the encapsulated and suspending fluids viscosities selects the TT or TB mode; only vesicle containing very viscous fluid tumbles [7]. This unusual dynamics of individual vesicles results in novel rheology: the effective viscosity of a dilute suspension of TT-vesicles decreases with the increasing viscosity of the inner fluid and exhibits a minimum at the TT–TB transition [8]. In contrast, emulsion viscosity monotonically increases with drop viscosity [9].

Thus far, all studies of vesicle dynamics have focused on a vesicle enclosing homogeneous fluid. However, eukaryotic cells contain nucleus and organelles (one notable exception are the mature red blood cells): The nucleus occupies 18% - 44% of the volume in human leukocytes [10] and affects leukocyte adhesion during inflammatory response [11]. RBCs infected with malaria parasites have reduced deformability which causes disruption (and even obstruction) of blood flow in the microcirculation [12], similar to the symptoms caused by sickle cell anemia [13]. One of the main causes for the impaired RBC deformability is the increased cytoplasmic viscosity due to parasites (in the case of malaria) or polymerized sickle hemoglobin (in sickle cell anemia).

A question naturally arises: Can we quantify the in-



crease of cytoplasmic viscosity due to internal structure? Does the inclusion introduce new features in the cell dynamics? In the case of double emulsion droplet (a viscous drop encapsulating another rigid particle or viscous drop), the hydrodynamic interactions between the enclosed particle and the confining interface destabilize and may cause a breakup of the aggregate [16]. In this Letter, we report the first study of the effect of an inclusion on vesicle behavior in shear flow. Using both theory and numerical simulations, we investigate the TT–TB transition and rheology of suspension of vesicles with a solid particle inside. We perform the small-deformation analysis in two dimensions and make detailed comparison with the two-dimensional simulation results. Analytical results from the three-dimensional theory confirm the general conclusions from the two-dimensional studies.

We consider a compound vesicle immersed in a linear shear flow  $\mathbf{U} = (\dot{\gamma}y, 0, 0)$  with  $\dot{\gamma}$  the constant shear rate. The deformable vesicle, in 2D, is characterized by the reduced area  $A^*$  (the ratio of the vesicle area  $A_0$  to the area of a circle with the vesicle circumference  $L_0$ ) and the inclusion filling fraction  $\phi = a^2\pi/A_0$ , where  $a$  is the inclusion equivalent-circle radius. The excess length  $\Delta_l \equiv L_0/\sqrt{A_0/\pi} - 2\pi = 2\pi(A^{*2} - 1)$ .

The velocity outside and inside the vesicle is governed by the incompressible Stokes equations, which are solved numerically by the Boundary Integral Method [17]. Focusing on cases where the interior and suspending fluids have the same viscosity (viscosity ratio  $\eta_{\text{in}}/\eta_{\text{out}} = 1$ ), the velocity  $\mathbf{v}(\mathbf{x})$  at any arbitrary point  $\mathbf{x}$  in the fluid can be

FIG. 2: Inclination angle  $\psi/\pi$  of a compound vesicle as a function of the inclusion filling fraction. The solid and dashed lines are the analytical result whereas the points are from simulations.

FIG. 3: Plot of the tank-treading frequency averaged over a period,  $\langle\omega\rangle$ , as a function of the filling fraction. Snapshots show the steady shapes. The lines are plotted to guide the eye.

written as

$$\mathbf{v}(\mathbf{x}) = \mathbf{U}(\mathbf{x}) + \mathcal{S}[\mathbf{f}_b + \mathbf{f}_\sigma](\mathbf{x}) + \mathcal{S}[\mathbf{f}](\mathbf{x}) + \mathcal{T}[\mathbf{u}](\mathbf{x}) \quad (1)$$

where  $\mathbf{U}$  is the imposed velocity,  $\mathbf{f}_b$  and  $\mathbf{f}_\sigma$  are membrane tractions,  $\mathbf{f}$  is the traction and  $\mathbf{u}$  is the velocity at the interface of the rigid inclusion.  $\mathcal{S}[\cdot]$  and  $\mathcal{T}[\cdot]$  are convolutions with the 2D Stokeslet and the Stresslet respectively [23]. The local inextensibility constraint requires the velocity along the membrane be solenoidal,  $\text{div}_\gamma(\mathbf{v}) = 0$ . This constraint introduces tension  $\sigma$  as a Lagrange multiplier [18]. Energy is required to bend the lipid membrane, and the membrane tractions are thus [14, 15]

$$\mathbf{f}_b = \kappa_B \left( c_{ss} + \frac{c^3}{2} \right) \mathbf{n}, \quad \mathbf{f}_\sigma = (\sigma \mathbf{x}_s)_s, \quad (2)$$

with  $\mathbf{n}$  the normal to the interface  $\gamma$ ,  $\kappa_B$  the bending rigidity,  $c$  the curvature, and  $s$  is the arclength parameter; subscript  $s$  denotes a derivative with respect to arclength.

In the limit of  $\mathbf{x}$  approaching the membrane interface, equation (1) gives an integro-differential equation for the evolution of the membrane. Similarly, taking the limit to the boundary of the rigid particle, we get an integral equation for the traction and velocity on the inclusion boundary. The system of equations is closed by the inextensibility constraint and the condition for a force-free and torque-free rigid body particle motion. We solve the coupled set of nonlinear integro-differential equations using a high-order time-marching scheme and a spectrally accurate spatial discretization scheme. More details of the numerical scheme can be found in [14, 19].

An example from our numerical simulations is shown in Figure 1, illustrating the dramatic changes the inclusion introduces in the interior flow. One feature is the formation of two vortices (seen at time 1.87). The interior flow streamlines for a particle-free vesicle are always circular. However, as the filling fraction (i.e. the inclusion size) increases it becomes inefficient to maintain a circulatory flow everywhere in the interior and the flow separates. Since the presence of the inclusion enhances dissipation, the compound vesicle behaves similarly to an inclusion-free vesicle encapsulating a higher viscosity fluid: The larger the inclusion size, the larger the effective interior fluid viscosity. Figures 2 and 3 show that indeed the inclination angle and the tank-treading frequency both reduce with increasing inclusion size. The TT-TB transition occurs when the steady inclination angle reaches zero, which gives a dependence of the critical

FIG. 4: Critical filling fraction ( $\phi_c$ ) versus reduced area  $A^*$  for tank-treading to tumbling transition obtained using boundary integral simulations, and the 2D and 3D analytical models.

filling fraction  $\phi_c$  on the vesicle reduced area. Figure 4 shows the boundary for TT-TB transition. For comparison, the TT-TB transition from the 3D analysis is plotted against the 3D reduced volume  $V^*$ .

In order to gain better physical insight and understand the hydrodynamic coupling of the inclusion dynamics and the confinement geometry (vesicle shape), we also developed analytical models for the compound vesicle dynamics in two- and three-dimensions. The 3D system is characterized by reduced volume  $V^* \equiv (1 + \Delta_a/4\pi)^{-3/2}$  (or excess area  $\Delta_a \equiv A_0/(3V_0/4\pi)^{2/3} - 4\pi$ ) and the filling fraction  $\phi = 4\pi a^3/3V_0$  with  $V_0$  the vesicle volume and  $A_0$  the vesicle area. In order to make analytical progress, we consider concentric configuration and vesicle shape close to a circle (in 2D) or a sphere (in 3D). In 2D, the nearly-circular vesicle shape is described by  $r = 1 + \sum_{n \neq 0} f_n e^{in\theta}$  with  $|f_n| \sim \mathcal{O}(\sqrt{\Delta_l})$ . The velocity field is expanded in basis of solutions of the Stokes equations  $\mathbf{v}_{nq}^\pm$  [24], where in 2D  $q = 0, 1$ ,

$$\mathbf{v} = \mathbf{U} + \sum_{nq} c_{nq} [\mathbf{v}_{nq}^\pm + \sum_{q'} X_{qq'}^n \mathbf{v}_{nq'}^-] \quad (3)$$

The scattering matrix  $X$  accounts for the flow perturbation due to the inclusion. Focusing on the  $n = \pm 2$  modes (the only modes that are excited by the external shear flow), the leading-order equations for the membrane deformation are (for details of the derivation see [24])

$$\dot{f} = g - \frac{3\beta}{\Delta_l} g f, \quad \dot{g} = -f - \frac{3\beta}{\Delta_l} g^2 + \beta, \quad (4)$$

where  $f_{\pm 2} = f \pm gi$ .  $\beta$  is a function of the inclusion radius  $a$ :

$$\beta = -\frac{\sqrt{2\pi}}{4} \frac{-1 + 3X_{00}^2 + X_{10}^2}{2 + 3X_{00}^2 - 3X_{01}^2 + X_{10}^2 - X_{11}^2} \xi, \quad (5)$$

$$\xi = 1 + X_{01}^2 + X_{11}^2 - \frac{(1 + X_{00}^2 + X_{10}^2)(-3 + 3X_{01}^2 + X_{11}^2)}{-1 + 3X_{00}^2 + X_{10}^2}, \quad (6)$$

where  $X_{00}^2 = a^4$ ,  $X_{01}^2 = 2a^6$ ,  $X_{10}^2 = -2a^4$ , and  $X_{11}^2 = -3a^4$ . A steady TT state corresponds to  $f = \Delta_l/3\beta$  and  $g^2 = \Delta_l/3(1 - \Delta_l/3\beta^2)$ . The TT inclination angle is  $\psi = -1/2 \arctan(g/f) = -1/2 \arctan(\sqrt{3\beta^2/\Delta_l - 1})$ . The critical filling fraction for TT-TB transition (which occurs when  $\psi = 0$ ) is computed from  $3\beta(\phi_c)^2 = \Delta_l$ . Good agreement in the inclination angle between numerical simulations and analysis is found for reduced area close to 1, while larger deviation is found for smaller reduced area, see Figure 2. This is also reflected in the TT-TB transition boundary (Figure 4). For an inclusion-free

FIG. 5: Effective interior fluid viscosity versus filling fraction  $\phi$ . Solid (dash-dotted) line is for 2D (3D) vesicle, and the dotted line is the effective interior viscosity from [22].

FIG. 6: Variation of effective shear viscosity  $T_{xy}$  versus the filling fraction for  $\Delta_l = 1.0$ . The inset shows  $N_1$  as a function of  $\phi$ .

2D vesicle, the critical viscosity ratio  $\lambda_c$  for the TT–TB transition is computed from  $3\pi/2(\lambda_c+1)^2 = \Delta_l$  [20]. The compound vesicle can be viewed as a membrane enclosing a homogeneous fluid with a higher viscosity due to the inclusion. The effective viscosity of the “equivalent fluid” can be estimated from the TT–TB transition: at  $\phi_c$ ,  $3\beta(\phi_c)^2 = 3\pi/2(\lambda_c+1)^2$ . Thus,  $\eta_{in}/\eta_{out} = \sqrt{\pi/2}/\beta - 1$ . The same estimate can be made for the 3D compound vesicle. Thus we find that if the inclusion takes 10% of the vesicle volume, the interior viscosity doubles (Figure 5), which is different from estimating the interior viscosity using the average shear viscosity of a suspension of rigid spheres without the confining membrane [22].

Next we explore the effect of the inclusion on the rheology of a dilute suspension of compound vesicles. Our numerical and analytical study shows that the steady effective bulk viscosity increases with the inclusion size. For a three-dimensional compound vesicle, the variation of the effective shear viscosity  $T_{xy}$  with the 3D filling fraction  $\phi$  is plotted in Figure 6 (see [24] for details of calculations). At a fixed reduced volume, both  $T_{xy}$  and the first normal stress  $N_1$  decrease with the filling fraction in the TT regime. In the TB and VB regimes, the averaged  $T_{xy}$  increases while  $N_1$  averages to 0. Close to the transition, the effective viscosity  $T_{xy}$  in the VB mode is lower than the TB mode value but eventually approaches it for large  $\phi$  (and hence large effective interior viscosity), which is significantly different from the inclusion–free vesicle case where the stresses in the VB and TB mode diverge as the interior fluid viscosity increases.

If the inclusion shape is non–spherical, the dynamics become more complex. For example, an ellipsoidal particle tumbles while the enclosing vesicle major axis oscillates around a non–zero inclination angle as seen in Figure 7. This motion resembles the swinging of RBC [21], but its mechanism is different. For RBCs the swinging arises from a periodic variation in the elastic membrane energy during tank treading. For compound vesicle the swinging is due to a periodic vesicle deformation as the tumbling inclusion pushes on the membrane. The “swinging” is more pronounced for larger inclusion size as seen by the increasing amplitude of the swings with the filling fraction.

To summarize, in this Letter we investigate the effect of an inclusion on vesicle behavior in linear shear flow. Particle dynamics in a confined geometry with dynamically evolving boundaries is a problem of fundamental interest, yet it is virtually unexplored. Our analytical theory

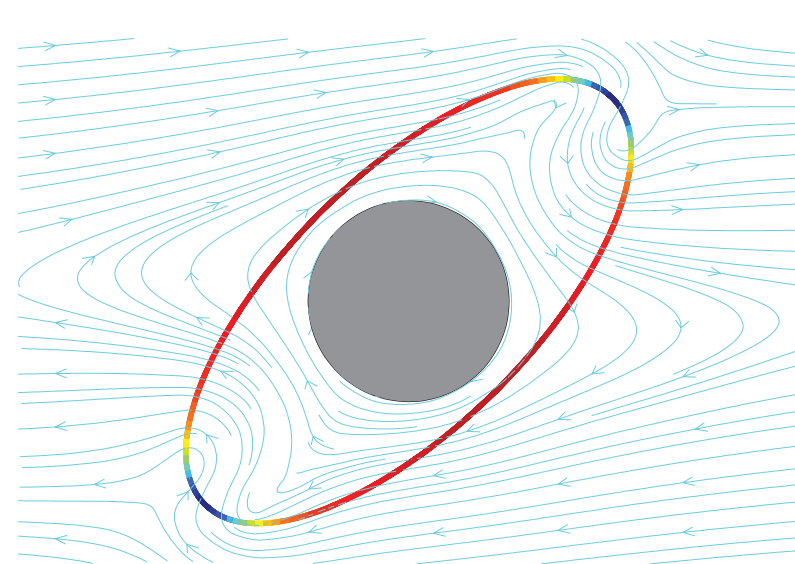
FIG. 7: Tank–treading vesicle with a tumbling elliptical inclusion.

and boundary integral simulations show that “internal” hydrodynamic interactions between the inclusion and the moving membrane induce TT–TB transition even if the inner and suspending fluids are the same and swinging in the presence of non–spherical inclusion. In a broader context, the results provide insights into the effects of internal structures such as the nucleus in leukocytes or parasites in malaria-infected erythrocytes on cell dynamics in microcirculatory flows. Multiple inclusions are expected to give rise to richer vesicle behavior, but pose greater challenge to numerical simulations [24]. We hope our study will stimulate further theoretical and experimental work on this interesting problem.

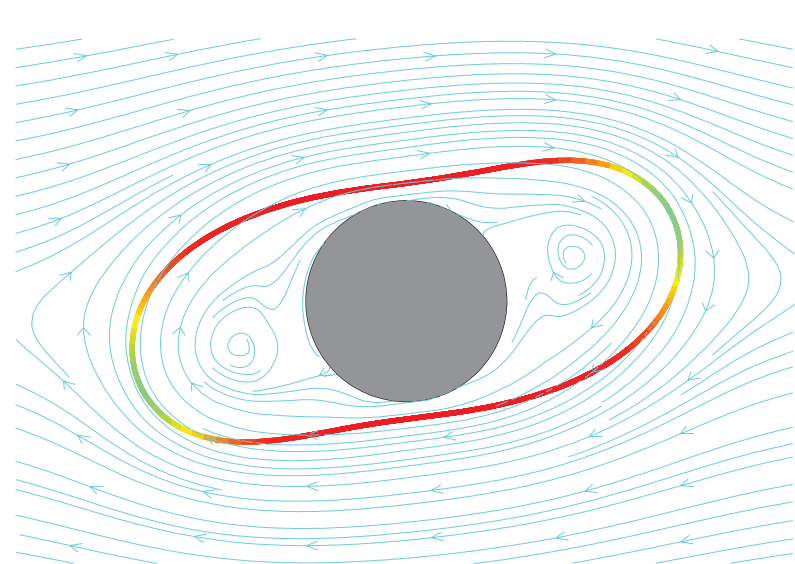
This work was supported by NSF (OCI-0749162, DMS-1009105, CBET-0853673, 0846247 and 093154).

- 
- [1] U. Seifert. *Advances in Physics*, 46:13, 1997.
  - [2] P. M. Vlahovska, T. Podgorski, and M. Misbah. *Comptes Rendus Physique*, 10:775, 2009; B. Kaoui and C. Misbah. *Phys. Rev. Lett.*, 103:188101, 2009; M. Abkarian and A. Viallat. *Soft Matter*, 4:653, 2008.
  - [3] V. Kantsler and V. Steinberg. *Phys. Rev. Lett.*, 95:258101, 2005; M.-A. Mader, V. Vitkova, M. Abkarian, A. Viallat, and T. Podgorski. *Eur. Phys. J. E*, 19:389, 2006.
  - [4] V. Kantsler and V. Steinberg. *Phys. Rev. Lett.*, 96:036001, 2006.
  - [5] J. Deschamps, V. Kantsler, and V. Steinberg. *Phys. Rev. Lett.*, 102:118105, 2009.
  - [6] H. Noguchi and G. Gompper. *Phys. Rev. Lett.*, 98:128103, 2007.
  - [7] C. Misbah. *Phys. Rev. Lett.*, 96:028104, 2006.
  - [8] G. Danker and C. Misbah. *Phys. Rev. Lett.*, 98:088104, 2007; V. Vitkova, M. Mader, B. Polack, C. Misbah, and T. Podgorski. *Biophys. J.*, 95:L33, 2008; V. Kantsler, E. Segre, and V. Steinberg. *Europhys. Lett.*, 82:58005, 2008.
  - [9] G. I. Taylor. *Proc. R. Soc. A*, 138:41, 1932.
  - [10] G. W. Schmid-Schonbein, Y. Y. Shih, and S. Chien. *Blood*, 56:866, 1980.
  - [11] N.A. N’Dri, W. Shyy, and R. Tran-Son-Tay. *Biophys. J.*, 85:2273, 2003.
  - [12] M. Diez-Silva, M. Dao, J. Han, C.T. Lim, and S. Suresh. *MRS BULLETIN*, 35:382, 2010.
  - [13] G.A. Barabino, M.O. Platt, and D.K. Kaul. *Annu. Rev. Biomed. Eng.*, 12:345, 2010.
  - [14] S. K. Veerapaneni, D. Gueyffier, D. Zorin, and G. Biros. *J. Comp. Phys.*, 228:2334, 2009;
  - [15] I. Cantat and C. Misbah. *Phys. Rev. Lett.*, 83:880, 1999.
  - [16] A. M. Davis and M. H. Brenner. *ASCE*, 107:609, 1981; H. A. Stone and L. G. Leal. *J. Fluid Mech.*, 211:123, 1990.
  - [17] C. Pozrikidis. *Boundary Integral and Singularity Methods for Linearized Viscous Flow*. Cambridge University Press, 1992.

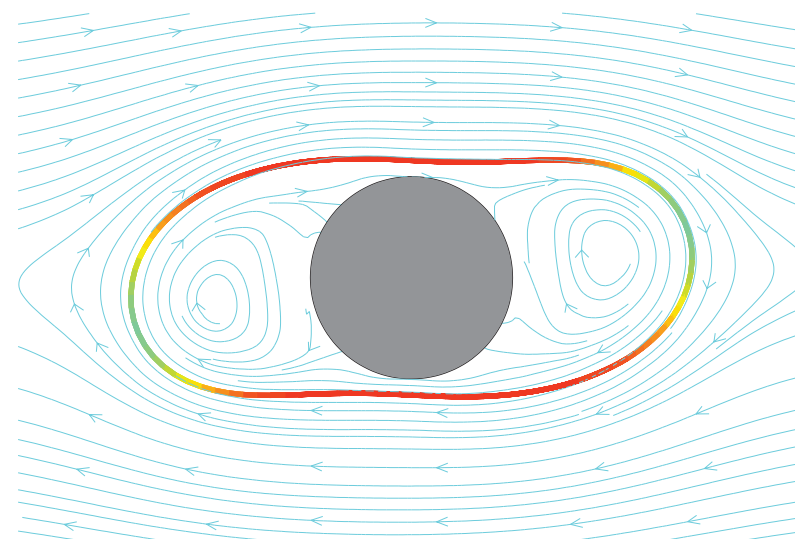
- [18] M. Kraus, W. Wintz, U. Seifert, and R. Lipowsky. *Phys. Rev. Lett.*, 77:3685, 1996.
- [19] A. Rahimian, S. K. Veerapaneni, and G. Biros. *J. Comp. Phys.*, 229:6466, 2010.
- [20] R. Finken, A. Lamura, U. Seifert, and G. Gompper. *Eur. Phys. J. E*, 25:309, 2008.
- [21] M. Abkarian, M. Faivre, and A. Viallat. *Phys. Rev. Lett.*, 98:188302, 2007; J. M. Skotheim and T. W. Secomb. *Phys. Rev. Lett.*, 98:078301, 2007.
- [22] C. G. de Kruif, E. M. F. van Iersel, and A. Vrij. *J. Chem. Phys.*, 83:4717, 1985.
- [23]  $\mathcal{S}[\mathbf{f}] = \frac{1}{4\pi\eta} \int_{\gamma} \left( -\log \|\mathbf{r}\| \mathbf{I} + \frac{\mathbf{r} \otimes \mathbf{r}}{\|\mathbf{r}\|^2} \right) \mathbf{f} d\gamma$  and  $\mathcal{T}[\mathbf{u}] = \frac{1}{\pi} \int_{\gamma} \frac{\mathbf{r} \otimes \mathbf{r}}{\|\mathbf{r}\|^4} (\mathbf{r} \cdot \mathbf{n}) \mathbf{u} d\gamma$  where  $\mathbf{r} = \mathbf{x} - \mathbf{y}$ ,  $\mathbf{n}$  is the normal to the interface  $\gamma$  and  $\mathbf{I}$  is the identity tensor.
- [24] See EPAPS Document No. X for details about the calculation. For more information on EPAPS see <http://www.aip.org/pubservs/epaps.html>



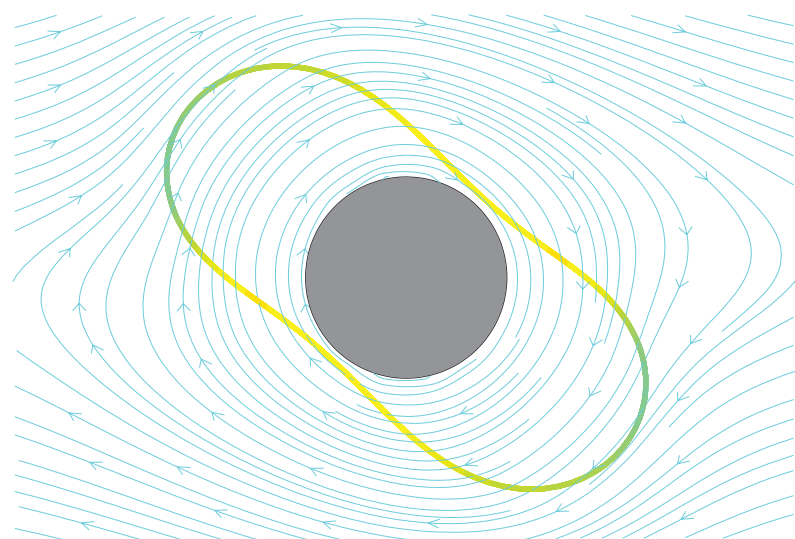
$t = 0.001$



0.68



1.87



5.00



-1.6

-1.4

-1.2

-1

-0.8

-0.6

-0.4

-0.2

0

0.2

